Aerosol and Air Quality Research

Synthesis of Cu-BTC Metal-Organic Framework for CO₂ Capture via Solvent-free Method: Effect of Metal Precursor and Molar Ratio

Pui San Ho[1], Kok Chung Chong[1,2*], Soon Onn Lai[1,2], Sze Sin Lee[1,2], Woei Jye Lau[3], Shih-Yuan Lu[4], Boon Seng Ooi[5]

[1] Department of Chemical Engineering, Lee Kong Chian Faculty of Engineering and Science, Universiti Tunku Abdul Rahman (UTAR), Jalan Sungai Long, Kajang 43000, Selangor, Malaysia
[2] Centre of Photonics and Advanced Materials Research, Universiti Tunku Abdul Rahman (UTAR), Kampar 31900, Perak, Malaysia
[3] Advanced Membrane Technology Research Centre (AMTEC), School of Chemical and Energy Engineering, Universiti Teknologi Malaysia, Johor Bahru 81310, Johor, Malaysia
[4] Department of Chemical Engineering, National Tsing Hua University, Hsinchu 30013, Taiwan
[5] School of Chemical Engineering, Engineering Campus, Universiti Sains Malaysia, Seri Ampangan, Nibong Tebal 14300, Pulau Pinang, Malaysia

ABSTRACT

The Cu-BTC (Copper-1,3,5-benzene tricarboxylate) is one of the representative metal organic frameworks (MOFs) that has shown outstanding performance for carbon dioxide (CO₂) adsorption. However, its conventional synthesis duration is relatively long, and the process requires the addition of bulk amounts of organic solvents. Herein, an enhanced solvent-free synthesis strategy was demonstrated in this work for the Cu-BTC synthesis. For this enhanced method, Cu-BTC was synthesized in 3 hours by mechanically grinding the mixture of copper (Cu) metal precursor and BTC organic linker without using solvent. The as-synthesized Cu-BTC samples were analyzed using various characterization techniques to examine and confirm their properties. The thermal stability result revealed that the self-synthesized Cu-BTC could sustain high temperature up to 290°C. Among the samples synthesized at different mole ratios, the Cu-BTC sample with the Cu to BTC mole ratio of 1.5:1 showed the highest BET surface area and the most significant pore volume of 1044 $m^2\,g^{-1}$ and 0.62 $cm^3\,g^{-1}$, respectively. Its CO₂ adsorption capacity was comparable with those fabricated using the solvent-based method, i.e., 1.7 mmol g^{-1} at 30°C and 1 bar. The results also showed that the synthesized Cu-BTC exhibited regenerative ability up to five adsorption-desorption cycles.

Keywords: Metal-organic framework, Cu-BTC, Solvent-free, Carbon dioxide, Adsorption

1 INTRODUCTION

Metal organic framework (MOF) is an organic-inorganic hybrid material with metal ions coordinated by organic linker molecules (Chen *et al.*, 2018). It has been identified as a promising adsorbent due to its high porosity, high surface area, good thermal stability, excellent pore volume and regeneration ability (Hong *et al.*, 2020; Pioquinto-García *et al.*, 2021). Furthermore, its surface properties, framework and pore structure can be easily tuned to fit specific applications (Zhou *et al.*, 2016; Kooti *et al.*, 2018). With all these features, MOF could overcome the limitations of rigid traditional adsorbents like zeolite or activated carbon. MOFs have also shown great potential for CO₂ adsorption (Ganesh *et al.*, 2014; Chen *et al.*, 2018).

Cu-BTC MOF, also known as HKUST-1 or MOF-199, is the representative MOF for CO₂ adsorption. It was firstly reported by Chui *et al.* (1999). This MOF is composed of dimer Cu coordinated to
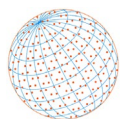
1,3,5-benzene tricarboxylate (BTC) with each copper ion linked to four oxygen atoms from the BTC molecule (Chen et al., 2018; Liu et al., 2018).

Many approaches had been reported in the past for Cu-BTC synthesis and these include conventional hydrothermal/solvothermal method (Chen et al., 2018; Morales et al., 2021), microwave-assisted method (McKinstry et al., 2017), sonication method (Lee et al., 2019) and electrochemical method (Lestari et al., 2016). Nevertheless, it must be pointed out that the conventional method for Cu-BTC preparation requires the use of organic solvent and long heating process ranging from hours to weeks (Chen et al., 2018; Morales et al., 2021). For instance, the HKUST-1-Ag$_3$PO$_4$/AgBr/Ag composite synthesized by Mosleh et al. (2017) required 24-h heating at 140°C. The synthesized composite was then used as a blue light-emitting diode light active photocatalyst. The Cu-BTC MOF synthesized by Liu et al. (2018) via hydrothermal meanwhile required 12-h heating at 120°C. Kaur and his co-workers prepared the Cu-BTC using hydrothermal method at 120°C for 20 hours and aimed to absorb methylene blue using the nanomaterial (Kaur et al., 2019). In the study by Anand et al. (2020), Cu-BTC was fabricated at lower temperature (85°C), but the duration was remained at 20 hours. Recently, Ediati and co-workers fabricated Cu-BTC with the addition of Al-MCM-41 for the application of methylene blue removal from an aqueous solution. In their work, the Cu-BTC was prepared by dissolving copper metal precursor in deionised water while BTC was dissolved in ethanol. The solution was then heated at 100°C for 10 hours followed by washing with methanol for three days (Ediati et al., 2021).

Based on these previous studies, it is well noted that the conventional method based on solvent is not environmentally friendly and consumes significant amount of energy. Moreover, the solvent added during the synthesis process is un-reusable and unrecyclable, which not only make the scaling-up production challenging, but also hinder the sustainable synthesis process.

Therefore, in this study, a solvent-free method is proposed for the sustainable synthesis of Cu-BTC. The proposed method can synthesize the Cu-BTC in 3 hours by employing mechanical force to grind the metal precursor and organic linker, forming MOF without requiring any solvent. Subsequently, the as-synthesized material was studied for its performance as CO_2 adsorbent. In addition, the effect of copper metal to BTC ligand ratio on Cu-BTC was investigated in terms of its physicochemical properties and CO_2 gas adsorption performance in this work.

2 METHODS

2.1 Chemicals

All chemicals used in this work are commercially available and used without further purification. Copper(II) nitrate trihydrate (99%, Acros Organics) was used as metal precursor, 1,3,5-benzenetricarboxylic acid (BTC) (98%, Acros Organics) as organic ligand and methanol (99.85+%, Fisher Chemical) as washing solvent.

2.2 Synthesis of Samples

Five different samples with varying Cu:BTC mole ratios (0.2:1, 0.5:1, 1:1, 1.5:1 and 2:1) denoted as M0.2, M0.5, M1, M1.5 and M2, respectively were prepared in this work (Table 1). Firstly, the weighted amount of copper(II) nitrate trihydrate and BTC were mixed and ground using mortar and pestle; the grinding process continued for 15 minutes. After that, the resulting mixture was transferred into a stainless-steel Teflon lined autoclave and heated at 120°C for 3 hours in a conventional oven. The sample was then let to cool down naturally to room temperature before

Table 1. Cu-BTC MOF samples synthesized in this work with varying copper to BTC mole ratios.

MOF Sample	Copper to BTC ratio	
	Copper	BTC
M0.2	0.2	1.0
M0.5	0.5	1.0
M1	1.0	1.0
M1.5	1.5	1.0
M2	2.0	1.0
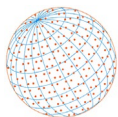
it was subjected to methanol washing for twice at 8,000-rpm centrifugation for 10 minutes to eliminate any unreacted reactants. Lastly, the sample was dried overnight in an oven at 80°C to obtain the final product in dark blue after activation.

2.3 Characterization Techniques

X-ray diffraction (XRD) patterns were obtained by employing Shimadzu Model 6000 diffractometer. All samples synthesized in this work were subjected to Cu-Kα radiation over 2θ from 5° to 40° with a scan speed of 1.2 degree min⁻¹. The crystallinity of samples can be determined by comparing the peak intensities of the sample based on the commercial MOF product, assuming the crystallinity of commercial MOF was 100%. The relative intensities of five characteristic planes, i.e., (200), (220), (222), (400) and (420) were calculated using the plane (222) as reference for each sample (Wijaya *et al.*, 2021). The crystallinity in percentage can be calculated using the formulae as follows (Mu *et al.*, 2018):

$$\text{Crystallinity } (\%) = \frac{\sum_{i=1}^{5} I_{sample}}{\sum_{i=1}^{5} I_{Basolite, C300}} \times 100 \tag{1}$$

Basolite C300, a commercial Cu-BTC MOF was used as a reference in the crystallinity calculation, the values of its peak intensity were obtained from (Mu *et al.*, 2018).

A Hitachi S-3400N scanning electron microscope (SEM) operated at an acceleration voltage of 15 kV was utilized to obtain the images of samples at different magnifications together with the energy-dispersive X-ray spectroscopy (EDX) analysis. The surface of samples was coated with a thin layer of conductive material (gold/platinum alloy) to improve the imaging prior to the SEM analysis.

Fourier transform infrared (FTIR) spectrum of respective sample was recorded by Nicolet iS10 instrument with wavenumber in the range of 400–4000 cm⁻¹. For the stability test, approximately 15 mg of sample was placed into a thermogravimetric analyzer (Perkin Elmer STA 8000). Each sample was exposed to an increment of temperature from 50°C up to 600°C, at a heating rate of 10°C min⁻¹ in a continuous flow of pure N_2 gas with its flow rate held constant at 20 mL min⁻¹ during the analysis.

Nitrogen adsorption/desorption test was carried out by a 3Flex Micromeritics surface characterization analyzer operated at 77 K. Initially, all samples were degassed at 150°C with N_2 gas purging to remove solvent or water from the samples. The surface textural properties, including Brunauer-Emmett-Teller (BET) surface area, micropore area, micropore volume and total pore volume were acquired from the N_2 adsorption/desorption analysis. BET specific surface area was used to determine from the N_2 adsorption isotherms in the relative pressure ranged from 0.005 to 0.05. At the same time, the total pore volume was calculated based on the single point adsorption at relative pressure (P/P_o) of 0.99. Additionally, the micropore area and micropore volume were determined by the t-plot method.

2.4 CO_2 Adsorption Test

The CO_2 adsorption capacity of samples was determined using TGA (Perkin Elmer STA 8000) at 30°C and at 1 bar. The adsorption test can be divided into two parts: degas and adsorption. Approximately 15 mg of sample was loaded onto TGA during the sample degasification stage. The temperature was set to increase from 50°C to 150°C with a heating rate of 10°C min⁻¹ in nitrogen gas flow and kept isothermal for 30 minutes at 150°C for removing moisture. Subsequently, the sample was cooled down to 30°C at a cooling rate of 5°C min⁻¹ and kept isothermally for another 15 minutes. After the sample temperature became stable at 30°C, the adsorption test began by switching the gas flow to CO_2 gas, and the adsorption continued for one hour. The adsorption capacity for each sample can be calculated using the formulae as follows:
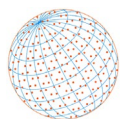
$$\text{Adsorption Capacity } \left(\text{mmol g}^{-1}\right) = \frac{\text{mass of adsorbed CO}_2 \left(\text{mg}\right) \big/ 44.009 \left(\text{mg mmol}^{-1}\right)}{\text{sample mass } \left(\text{g}\right)} \qquad (2)$$

In order to test the reusability of Cu-BTC MOF synthesized in this work, a CO_2 cyclic adsorption-desorption test was performed for the sample with the highest CO_2 adsorption capacity in the CO_2 adsorption test. In the desorption test, N_2 was used to purge off the adsorbed CO_2 in the sample with an elevated temperature of 100°C. The adsorption followed by the desorption process was repeated five cycles to examine the sample's regeneration ability. The regenerative performance in percentage can be determined using the equation as follows:

$$\text{Regenerative } \left(\%\right) = 1 - \frac{\text{Adsorption capacity 1}^{\text{st}} \text{ cycle} - \text{Adsorption capacity 5}^{\text{th}} \text{ cycle}}{\text{Adsorption capacity 1}^{\text{st}} \text{ cycle}} \times 100 \qquad (3)$$

The flow rate of CO_2 and N_2 were set at 20 mL min^{-1} in both the CO_2 adsorption test and regeneration test.
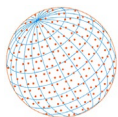
3 RESULTS AND DISCUSSION

3.1 Characterization of Cu-BTC

The as-synthesized Cu-BTC sample was in light blue, but the colour was changed to dark blue after being activated by methanol as shown in Fig. 1. Our results are in good agreement with other works that employed conventional solvent method to synthesize Cu-BTC (Al-Janabi et al., 2015; Chen et al., 2018; Nobar, 2018). The colour change was due to the elution of coordinated solvent or water from copper sites, reducing the copper coordination number from six to four (Cheng et al., 2009). It must be pointed out that the colour change is reversible, and the dark-blue sample could turn to light blue once it is exposed to a humidity atmosphere.

XRD patterns for Cu-BTC samples with different Cu to BTC molar ratios synthesized in this work are presented in Fig. 2(a). It can be observed that the XRD patterns of M0.5, M1, M1.5 and M2 were similar in which they showed three prominent distinctive peaks at 2θ of 9.5°, 11.6° and 13.4°. These peaks were in accordance with the simulated XRD pattern for HKUST-1 and also matched with the XRD results for Cu-BTC synthesized by solvothermal method (Yan et al., 2014; Al-Janabi et al., 2015; Liu et al., 2018; Souza et al., 2019). Thus, it can be confirmed that Cu-BTC was successfully synthesized using the solvent-free method. The XRD pattern for M0.2 was different from other samples. Based on Fig. 2(b), the XRD pattern for M0.2 was similar to the pure BTC, suggesting that the Cu-BTC was not really formed using starting materials with copper metal to BTC molar ratio of 0.2 to 1.
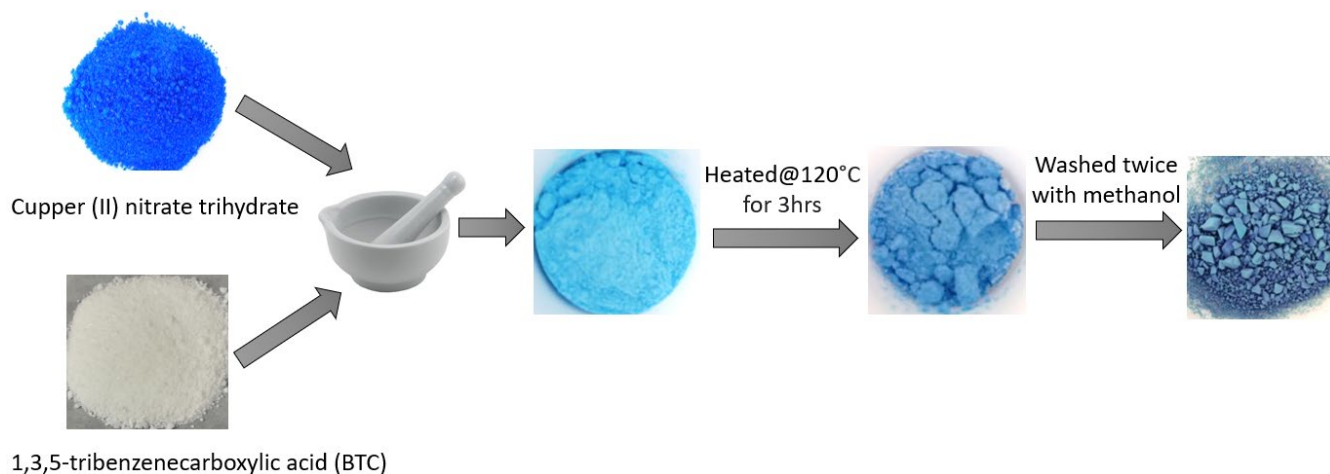
**Fig. 1.** Colour changes of Cu-BTC along with its synthesis and activation process.
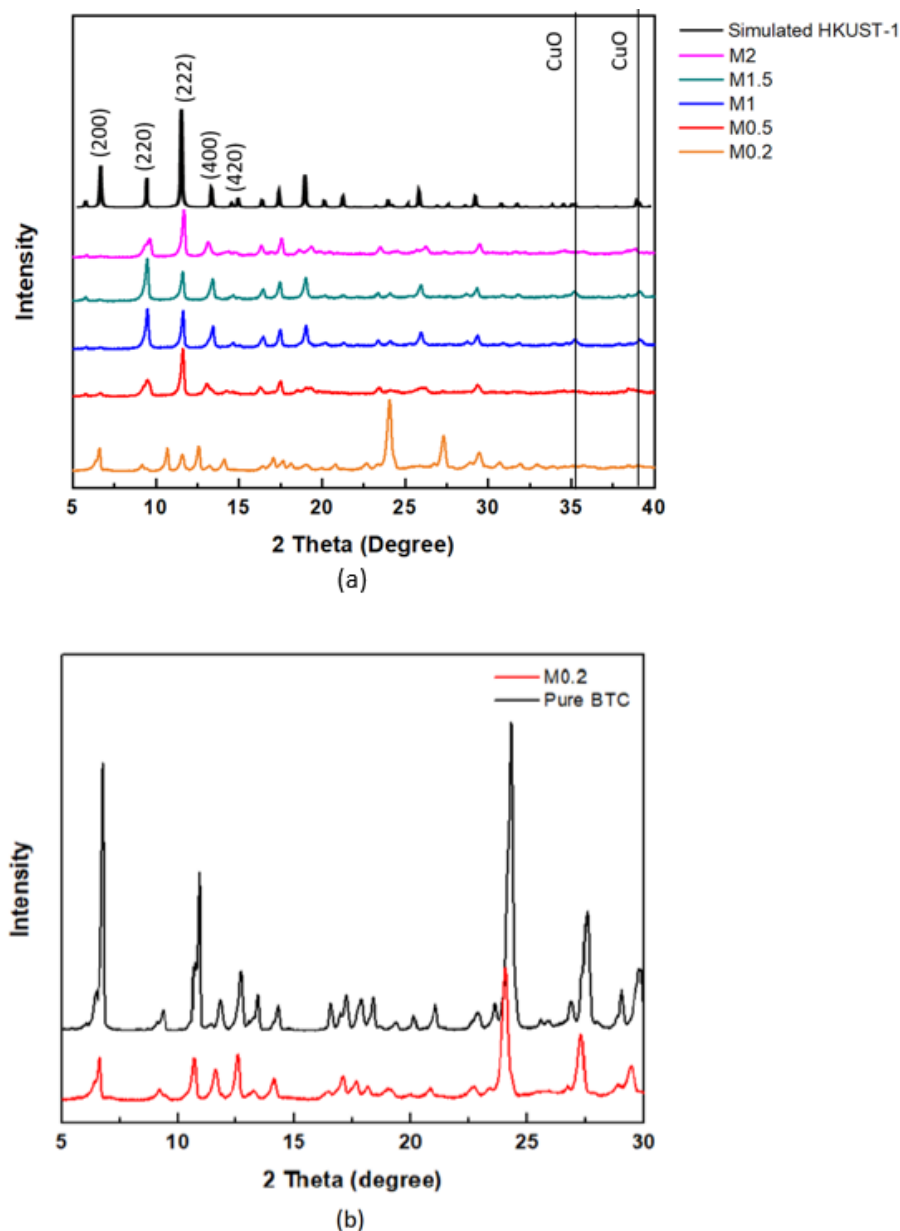
Fig. 2. (a) XRD patterns of Cu-BTC samples with different copper to BTC molar ratios synthesized in this work and (b) comparison between XRD pattern of M0.2 with pure BTC organic ligand.

The formed Cu-BTC was reported to contain impurities such as CuO and Cu_2O (Nobar, 2018). The presence of these impurities can be determined from the XRD pattern. 2θ at around 35.5° and 38.7° implied the existence of CuO while 36.43° was corresponded to Cu_2O (Nobar, 2018). By looking at the XRD results shown in Fig. 2(a), some small peaks can be observed at 35.2° (for M1 and M1.5) and 39° (for M1, M1.5 and M2), indicating the presence of trace CuO for the M1, M1.5 and M2. While the characteristics peak for Cu_2O was not detected in any XRD graphs in Fig. 2(a).

The peak intensities of Cu-BTC samples synthesized in this work were extracted from the XRD result and listed in Table 2. According to Table 2, M1, M1.5 and M2 provided a crystallinity percentage larger than 100%, implying that the Cu-BTC synthesized using the proposed method exhibited a higher crystallinity degree than that of the commercial MOF - Basolite C300. The M1.5 possessed the highest crystallinity with 30% more than the Basolite C300.

SEM images for the samples with different copper to BTC molar ratios as starting materials are shown in Fig. 3. Different morphology was observed for sample M0.2 in Fig. 3(a); it consisted of
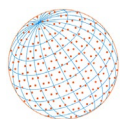
Table 2. Relative peak intensities based on peak intensities of plane (222) and crystallinity percentage of Cu-BTC synthesized in this work.

Sample Name	I(200) (%)	I(220) (%)	I(222) (%)	I(400) (%)	I(420) (%)	Crystallinity (%)
M0.5	14.5	27.2	100	21.8	13.2	90.8
M1	15.4	46.7	100	44.1	19.5	115.9
M1.5	15.3	62.9	100	54.3	20.8	130
M2	15.1	40.9	100	35.6	24.5	111
Basolite C300	16	47.6	100	27.4	3.8	100
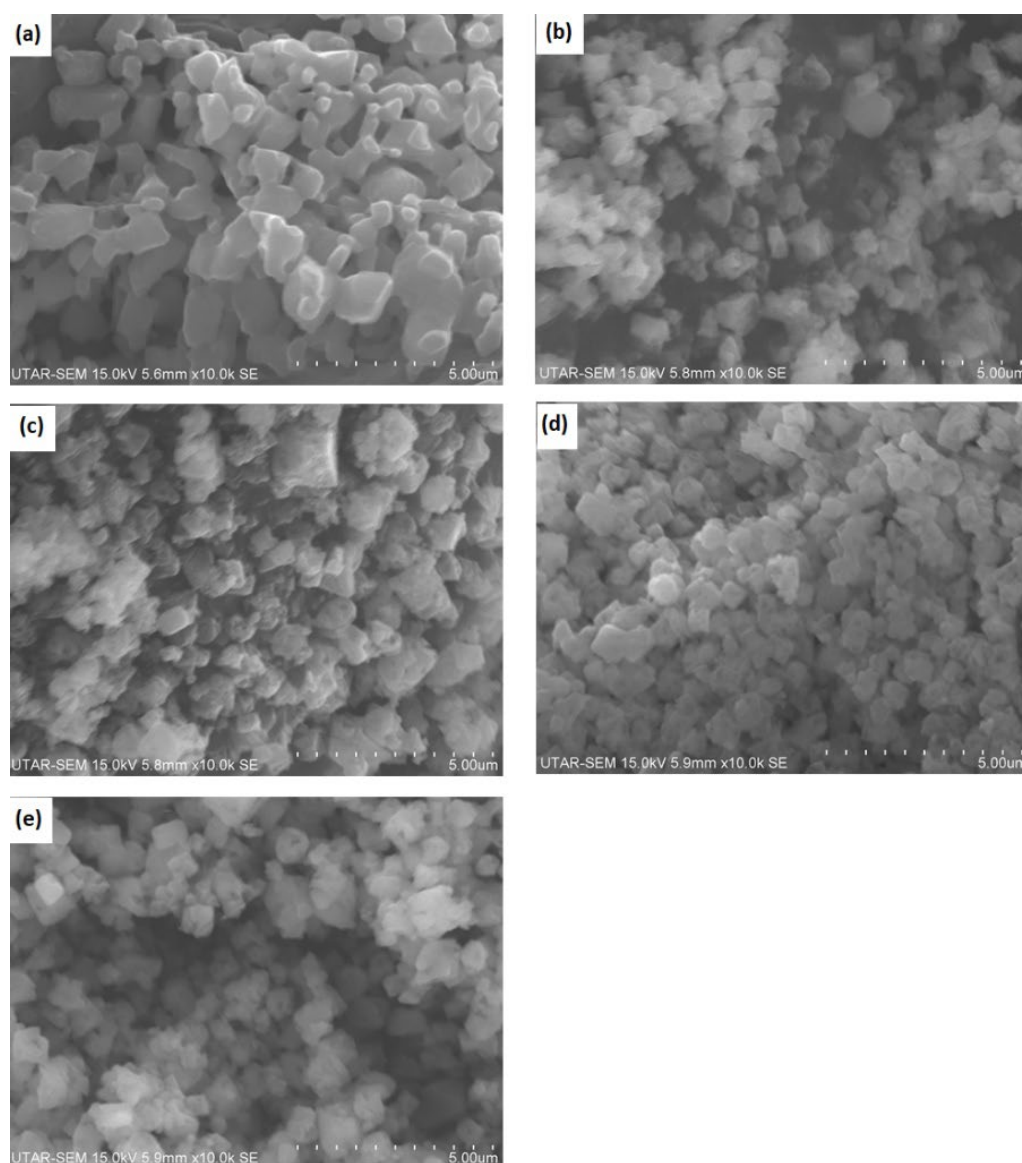
Fig. 3. SEM images of (a) M0.2, (b) M0.5, (c) M1, (d) M1.5 and (e) M2.

irregularly shaped particles with a bigger average size of *ca.* 20 µm. In combination with the XRD result, it was evident that Cu-BTC was unable to form under the reaction condition of Cu to BTC molar ratio of 0.2 to 1 using this method. By looking at the SEM images of M0.5, M1, M1.5 and M2 (Figs. 3(b–e)), no significant morphological difference was observed. All samples exhibited well-defined octahedrons with a particle size ranging from 5 to 15 µm, which was consistent with the morphology of Cu-BTC (synthesized by solvothermal method) reported elsewhere (Al-Janabi *et al.*, 2015; Mahadi *et al.*, 2016; Chen *et al.*, 2018; Nobar, 2018).
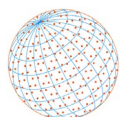
EDX analysis results for Cu-BTC samples synthesized in this work are presented in Table 3. The incorporation of the copper metal element within the samples regardless of the metal-to ligand ratio was evidenced by the EDX result. At the same time, the C and O elements were originated from the BTC organic linker.

The FTIR spectra of M0.5, M1, M1.5 and M2 as shown in Fig. 4 were very consistent with other studies which synthesized the Cu-BTC based on solvent method (Morales *et al.*, 2021; Wang *et al.*, 2022). The absorption bands at 490 cm^{-1} and 730 cm^{-1} were attributed to Cu-O stretching vibration characteristics (Goyal *et al.*, 2022). Strong peaks observed at around 1374 cm^{-1} and 1448 cm^{-1} were due to the symmetric stretching of the carboxylate group (COOH) within the BTC. In comparison, the absorption bands in the range of 1550–1645 cm^{-1} were corresponded to the asymmetric stretching of COOH (Morales *et al.*, 2021; Goyal *et al.*, 2022). The broadband in the region of 2700–3600 cm^{-1} was ascribed to the presence of hydroxyl group of carboxylic acid (BTC) and the adsorbed water within the samples (Thi *et al.*, 2013).
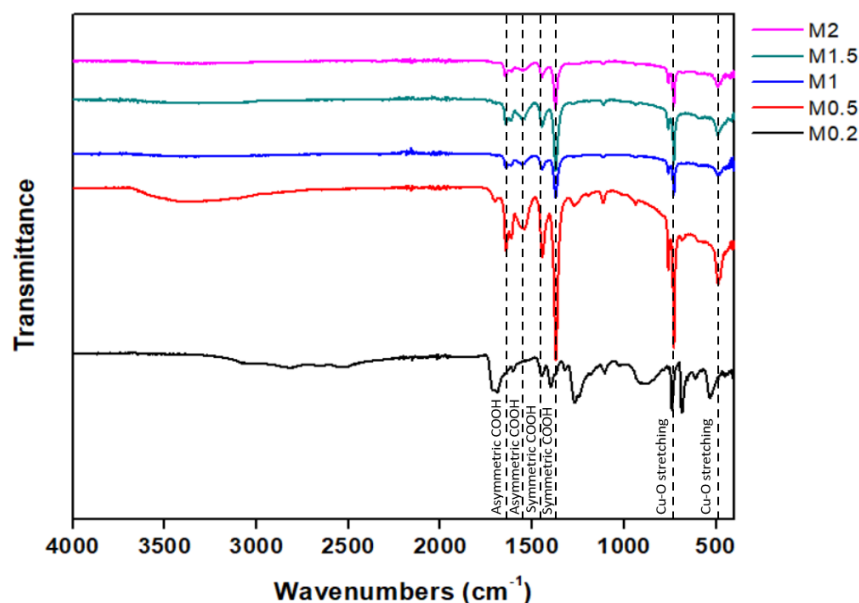
3.2 Textural Properties of Cu-BTC

Surface analysis of Cu-BTC is important as its textural properties play a dominant role in determining their performance in CO_2 adsorption (Wang *et al.*, 2022). Fig. 5 shows N_2 adsorption and desorption isotherms of different Cu-BTC carried out at 77 K. The isotherm of M0.2 exhibited a plateau with almost no N_2 adsorption, suggesting its non-porous structure. For this sample, Cu-BTC was not able to form owing to the low Cu to BTC mole ratio (0.2 to 1) as confirmed by the XRD and SEM results.

According to the IUPAC classification, the isotherms displayed by M0.5-M2 belong to Type I(a). This is because the N_2 adsorption equilibrium was rapidly reached in the low P/P$_o$ region, and the adsorption/desorption branches coincided well without an obvious hysteresis loop (Pan *et al.*, 2021; Li *et al.*, 2021). The reversible Type I(a) was of the physisorption isotherm for micropores dominant solids (Thommes *et al.*, 2015).

Table 3. The elemental composition of Cu-BTC synthesized in this work.

Sample	Cu:BTC Molar Ratio	Cu (wt%)	C (wt%)	O (wt%)
M0.5	0.5:1	23.46	46.65	29.89
M1	1:1	28.92	39.17	31.91
M1.5	1.5:1	30.11	41.59	28.30
M2	2:1	28.61	40.17	31.22

Fig. 4. FTIR spectra of Cu-BTC samples synthesized in this work.

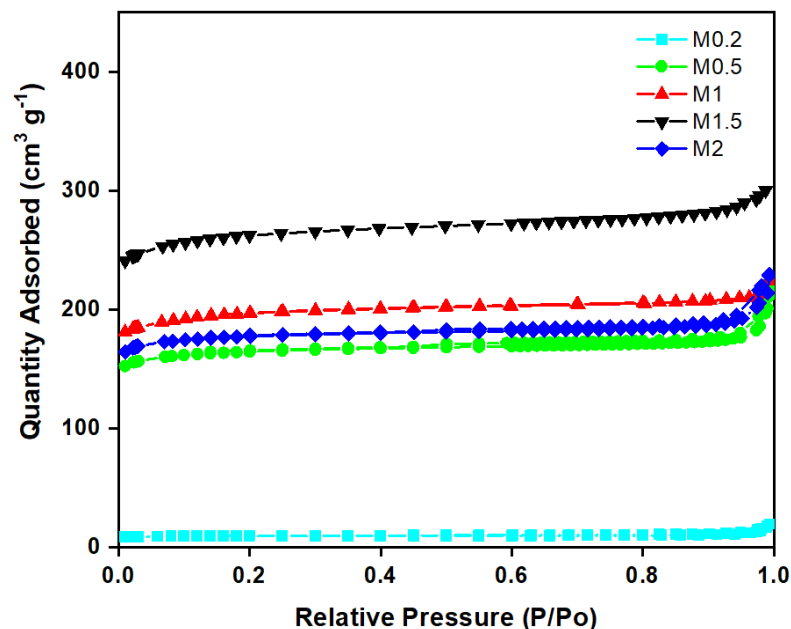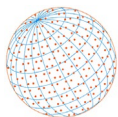**Fig. 5.** N_2 adsorption and desorption isotherms of Cu-BTC MOF synthesized in this work.

Table 4. Textural properties of Cu-BTC MOFs synthesized in this work[a].

Sample Name	S_{BET} (m^2 g^{-1})	$S_{Micropore}$ (m^2 g^{-1})	$V_{total pore}$ (cm^3 g^{-1})	$V_{Micropore}$ (cm^3 g^{-1})
M0.5	662.5	599.9	0.34	0.23
M1	780.4	683.9	0.35	0.26
M1.5	1044.0	940.0	0.62	0.36
M2	716.7	653.6	0.36	0.25

[a] S_{BET}: specific surface area obtained by BET equation at P/Po range from 0.005 to 0.05; $S_{Micropore}$: Micropore area and $V_{Micropore}$: Micropore volume calculated by t-plot method; $V_{total pore}$: Total pore volume calculated based on single-point N_2 adsorption at P/Po: ~0.99.

The textural properties, including the BET surface area, micropore area, total pore volume and micropore volume of Cu-BTC samples synthesized in this work are summarized in Table 4. The surface area and pore volume increased with increasing the Cu to BTC mole ratio from 0.2:1 to 1.5:1. The M1.5 possessed the most desired textural properties compared to the other samples synthesized. It showed the highest BET surface area (1044 m^2 g^{-1}) and micropore area (940 m^2 g^{-1}) together with a great pore volume (0.62 cm^3 g^{-1}). By further increasing the ratio to 2:1, the surface area and pore volume decreased correspondingly, indicating the importance of proper manipulation of the Cu to BTC mole ratio in synthesizing the desired Cu-BTC framework. The textural properties of Cu-BTC synthesized in this work are comparable to those synthesized using the conventional solvent method with the surface area normally range from 700 to 1000 m^2 g^{-1} and pore volume of around 0.7 cm^3 g^{-1} (Al-Janabi *et al.*, 2015).

3.3 Thermal Stability Test

Fig. 6 compares the thermal stability of different Cu-BTC samples. The Cu-BTC synthesized in this work experienced three stages of weight loss when exposing to high temperature, which is similar to those samples synthesized by solvothermal method (Yan *et al.*, 2014; Goyal *et al.*, 2022). About 15% of weight loss happened in the stage I (below 130°C) and this was due to the desorption of embedded water and guest molecules (Goyal *et al.*, 2022). A plateau was observed in the stage II (from 130°C to 290°C), indicating the Cu-BTC samples synthesized in this work were stable in this temperature range (Yan *et al.*, 2014). The framework structure of the material was in decomposition from 290°C onwards as evidenced by sharp weight loss occurring between 290°C and 350°C. After the decomposition at 350°C, the structure of Cu-BTC samples were completely
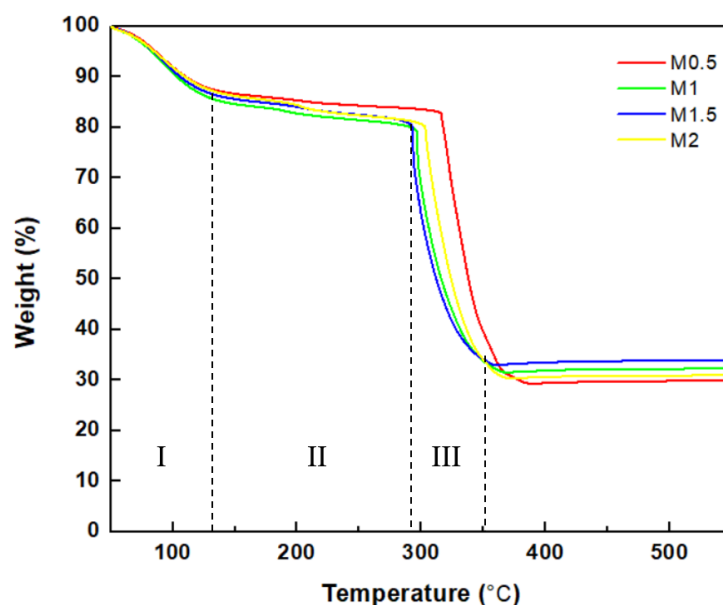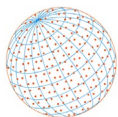
Fig. 6. TGA curves of Cu-BTC MOFs synthesized in this work.

collapsed and transformed into the residuals of copper oxides (CuO and Cu_2O), copper metal (Cu) and carbon compounds (CO and CO_2) (Salehi and Anbia, 2017; Mu *et al.*, 2018). The final residual weight for M1.5 was the highest, which is 33.91%. It was followed by M1, M2 and M0.5. This observation can be correlated to the EDX analysis result, where the Cu element composition for the M1.5 was the highest followed by the M1, M2 and M0.5, since the remaining residual mainly made up of the copper metal or cupper oxides compounds. In general, the Cu-BTC synthesized using the proposed solvent-free method exhibited relatively good thermal stability by maintaining the MOF structure up to 290°C.

3.4 CO$_2$ Adsorption Performance

The CO_2 adsorption on the Cu-BTC samples was further tested using a TGA at 30°C and the results are shown in Fig. 7. As can be seen, the M0.2 showed a plateau in its CO_2 adsorption isotherm, indicating no adsorption taking place for this sample. For M0.5, M1, M1.5 and M2, their CO_2 adsorption isotherms approached equilibrium after 1-h adsorption test. The CO_2 adsorption capacity for M0.5 was 1.2 mmol g^{-1}. When the Cu to BTC mole ratio increased from 0.5:1 to 1.5:1, the CO_2 adsorption capacities improved. M1.5, with the most outstanding textural properties, achieved the highest CO_2 adsorption capacity up to 1.7 mmol g^{-1}. However, by further increasing the Cu to BTC mole ratio from 1.5:1 to 2:1, the CO_2 adsorption capacity of M2 dropped to 1.4 mmol g^{-1}.

Table 5 compares the CO_2 adsorption capacity of self-synthesized Cu-BTC with other types of MOFs such as MIL-101(Cr), ZIF-88 and UiO-66(Ce) reported in the literature. Our solvent-free synthesized Cu-BTC (M1.5) was found to achieve the highest CO_2 adsorption capacity of 1.7 mmol g^{-1}, which was relatively high compared to the conventionally synthesized Cu-BTC and other MOFs. The CO_2 adsorption of M1.5 however was slightly lower compared to other studies (Ganesh *et al.*, 2014; Zhao *et al.*, 2014; Mu *et al.*, 2018). We believed the lower performance was due to the variation of adsorption conditions employed. Since adsorption conditions might affect the adsorption capacity, the CO_2 adsorption kinetic is favourable to low temperature but high pressure (Yang *et al.*, 2014).

Fig. 8 reveals the relationship between the CO_2 adsorption capacity and the textural properties of Cu-BTC MOF synthesized in this work. It is generally accepted that the textural properties influence the CO_2 adsorption performance and high surface area and pore volume are favourable for the adsorption mechanism (Chen *et al.*, 2014). It was noteworthy to observe that in Fig. 8, the higher the surface area and pore volume of Cu-BTC, the higher the CO_2 adsorption capacity achieved and vice versa. The observed trend was in line with the findings of other reported works (Chen *et al.*, 2018; Nobar, 2018; Yulia *et al.*, 2019). Moreover, the textural properties of Cu-BTC synthesized in this work were found to be in line with the result of CO_2 adsorption capacity.
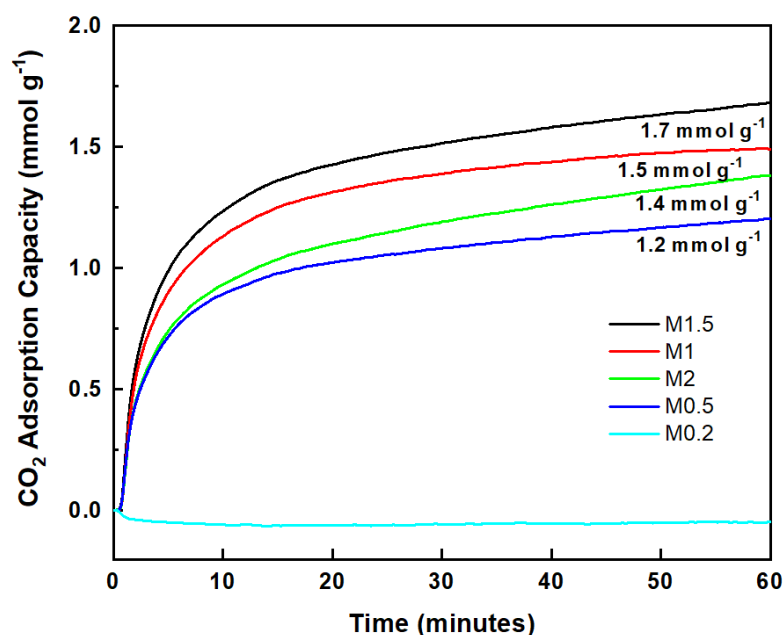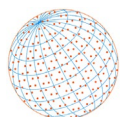
Fig. 7. CO_2 adsorption isotherms of samples synthesized in this work.

**Table 5.** Comparison of CO_2 adsorption capacity of Cu-BTC with other studies.

| Sample name	Pressure (bar)	Temperature (°C)	CO_2 adsorption capacity (mmol g^{-1})	Synthesis Method	References
Cu-BTC	1	25	1.526	solvothermal	(Shang *et al.*, 2020)
Cu-BTC	1	30	1.45	solvothermal	(Souza *et al.*, 2019)
Cu-BTC	5	32	1.8	solvothermal	(Zhao *et al.*, 2014)
Cu-BTC	1	27	1.84	solvothermal	(Mu *et al.*, 2018)
Cu-BTC	1	30	1.7	solvent-free	This work
MIL-101(Cr)	10	30	1.17	solvothermal	(Ye *et al.*, 2013)
ZIF-88	1	25	0.76	solvothermal	(McEwen *et al.*, 2013)
UiO-66(Ce)	1	25	0.9011	solvothermal	(Stawowy *et al.*, 2019)
Zr-fumarate	1	25	1.818	solvothermal	(Ganesh *et al.*, 2014)

3.5 Regeneration Test

CO_2 adsorption-desorption test was further conducted on the best performing M1.5 sample to study its reversibility and regenerative ability and the results are presented in Fig. 9. After each adsorption test, regeneration was accomplished by elevating the temperature to 100°C with N_2 gas flow. The adsorption-desorption test was repeated for 5 cycles. After 5 cycles of regeneration, the CO_2 adsorption capacity for M1.5 was reported to drop from 1.11 to 0.88 mmol g^{-1}, accounting for ~20% reduction in performance. In other words, its CO_2 adsorption performance could still retain up to 80% after 5 cycles of regeneration, implying its reusability for at least 5 cycles.

4 CONCLUSIONS

In this study, we demonstrated an enhanced solvent-free approach to synthesize the Cu-BTC for potential use in CO_2 adsorption. It was discovered that the proper manipulation of Cu to BTC mole ratio in synthesizing Cu-BTC was important as it could greatly affect its formation and textural properties. Among the mole ratios tested, the Cu to BTC mole ratio of 1.5:1 appeared to be the most suitable mole ratio for the synthesis of Cu-BTC as the M1.5 was able to achieve high specific surface area (1044 m^2 g^{-1}) and attain the most promising CO_2 adsorption capacity (1.7 mmol g^{-1}). Additionally, this sample also showed excellent regenerative performance as it could be reused
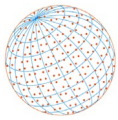
for at least 5 cycles with minimum drop in its adsorption capacity. Hence, it is concluded that the Cu-BTC synthesized in this work via the solvent-free method is worth further study as potential sorbent for CO_2 capture and storage.
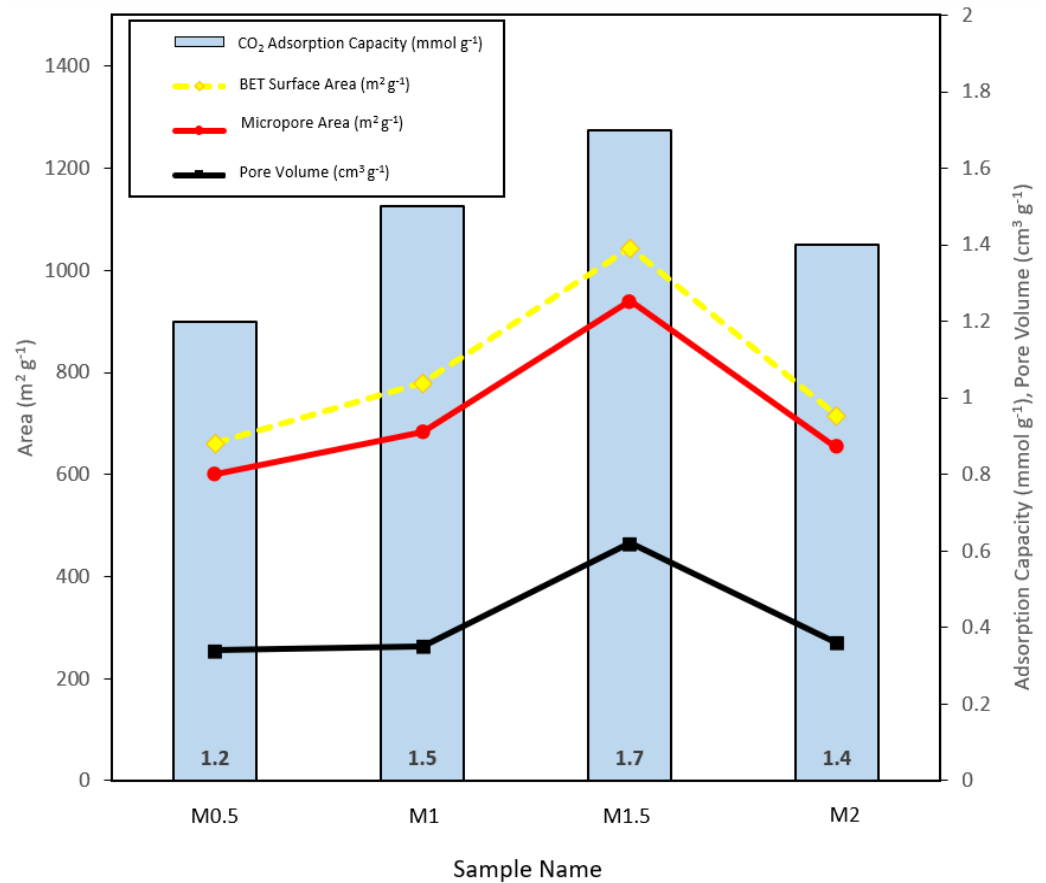
Fig. 8. The relationship between the CO_2 adsorption capacity and the textural properties of Cu-BTC MOFs synthesized in this work.

(a)

(b)
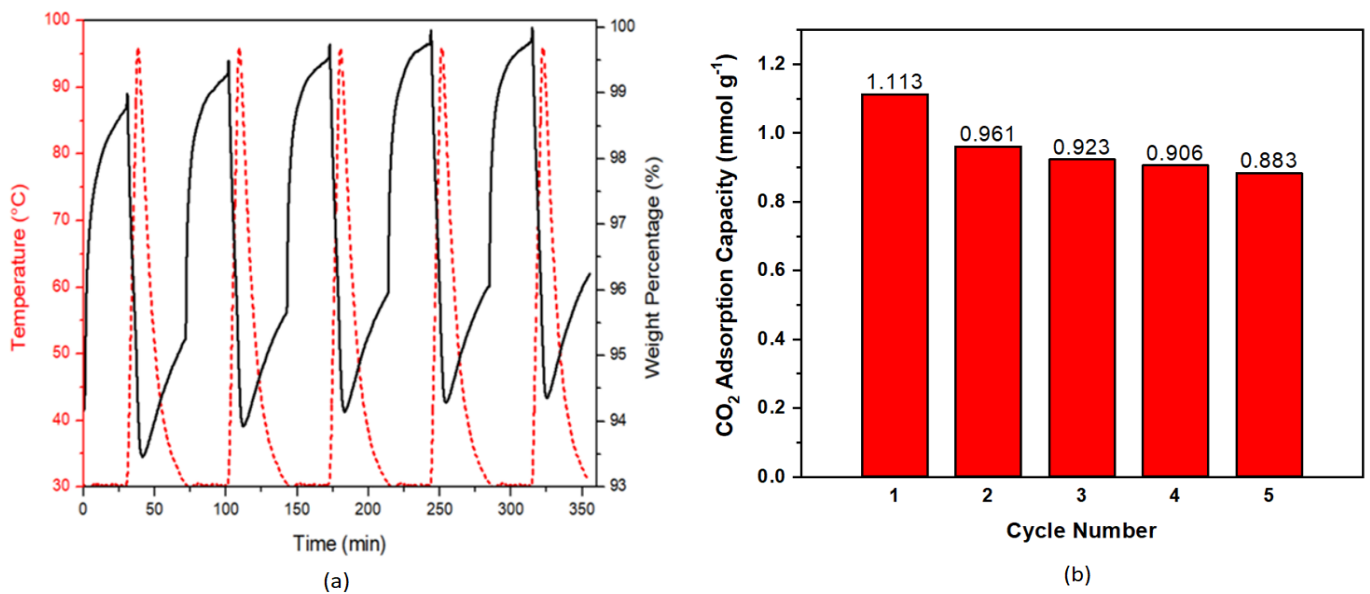
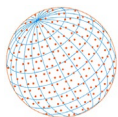**Fig. 9.** (a) Regeneration test isotherm for M1.5. (b) CO_2 adsorption capacity of each adsorption-desorption cycle for M1.5.
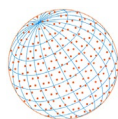
ACKNOWLEDGMENTS

REFERENCES

Al-Janabi, N., Hill, P., Torrente-Murciano, L., Garforth, A., Gorgojo, P., Siperstein, F., Fan, X. (2015). Mapping the Cu-BTC metal–organic framework (HKUST-1) stability envelope in the presence of water vapour for CO_2 adsorption from flue gases. Chem. Eng. J. 281, 669–677. https://doi.org/10.1016/j.cej.2015.07.020

Anand, B., Younis, S.A., Szulejko, J.E., Kim, K.H., Zhang, W. (2020). The potential utility of HKUST-1 for adsorptive removal of benzene vapor from gaseous streams using a denuder versus a packed-bed adsorption system. J. Cleaner Prod. 275, 122359. https://doi.org/10.1016/j.jclepro.2020.122359

Chen, L.C., Peng, P.Y., Lin, L.F., Yang, T.C.K., Huang, C.M. (2014). Facile preparation of nitrogen-doped activated carbon for carbon dioxide adsorption. Aerosol Air Qual. Res. 14, 916–927. https://doi.org/10.4209/aaqr.2013.03.0089

Chen, Y., Mu, X., Lester, E., Wu, T. (2018). High efficiency synthesis of HKUST-1 under mild conditions with high BET surface area and CO_2 uptake capacity. Prog. Nat. Sci.: Mater. Int. 28, 584–589. https://doi.org/10.1016/j.pnsc.2018.08.002

Cheng, Y., Kondo, A., Noguchi, H., Kajiro, H., Urita, K., Ohba, T., Kaneko, K., Kanoh, H. (2009). Reversible structural change of Cu-MOF on exposure to water and its CO_2 adsorptivity. Langmuir 25, 4510–4513. https://doi.org/10.1021/la803818p

Chui, S.S.Y., Lo, S.M.F., Charmant, J.P.H., Orpen, A.G., Williams, I.D. (1999). A chemically functionalizable nanoporous material $[Cu_3(TMA)_2(H_2O)_3]_n$. Science 283, 1148–1150. https://doi.org/10.1126/science.283.5405.1148

Ediati, R., Laharto, P.B.F., Safitri, R., Mahfudhah, H., Oktavia Sulistiono, D., Denisa Syukrie, T., Nadjib, M. (2021). Synthesis of HKUST-1 with addition of Al-MCM-41 as adsorbent for removal of methylene blue from aqueous solution. Mater. Today:. Proc. 46, 1799–1806. https://doi.org/10.1016/j.matpr.2020.06.361

Ganesh, M., Hemalatha, P., Peng, M.M., Cha, W.S., Jang, H.T. (2014). Zr-fumarate MOF a novel CO_2-adsorbing material: synthesis and characterization. Aerosol Air Qual. Res. 14, 1605–1612. https://doi.org/10.4209/aaqr.2013.11.0337

Goyal, P., Paruthi, A., Menon, D., Behara, R., Jaiswal, A., Keerthy, V., Kumar, A., Krishnan, V., Misra, S.K. (2022). Fe doped bimetallic HKUST-1 MOF with enhanced water stability for trapping Pb(II) with high adsorption capacity. Chem. Eng. J. 430, 133088. https://doi.org/10.1016/j.cej.2021.133088

Hong, W.Y., Perera, S.P., Burrows, A.D. (2020). Comparison of MIL-101(Cr) metal-organic framework and 13X zeolite monoliths for CO_2 capture. Microporous Mesoporous Mater. 308, 110525. https://doi.org/10.1016/j.micromeso.2020.110525

Kaur, R., Kaur, A., Umar, A., Anderson, W.A., Kansal, S.K. (2019). Metal organic framework (MOF) porous octahedral nanocrystals of Cu-BTC: Synthesis, properties and enhanced adsorption properties. Mater. Res. Bull. 109, 124–133. https://doi.org/10.1016/j.materresbull.2018.07.025

Kooti, M., Pourreza, A., Rashidi, A. (2018). Preparation of MIL-101-nanoporous carbon as a new type of nanoadsorbent for H_2S removal from gas stream. J. Nat. Gas Sci. Eng. 57, 331–338. https://doi.org/10.1016/j.jngse.2018.07.015

Lee, J.E., Kim, D.Y., Lee, H.K., Park, H.J., Ma, A., Choi, S.Y., Lee, D.S. (2019). Sonochemical synthesis of HKUST-1-based CuO decorated with Pt nanoparticles for formaldehyde gas-sensor applications. Sens. Actuators, B 292, 289–296. https://doi.org/10.1016/j.snb.2019.04.062

Lestari, W.W., Adreane, M., Purnawan, C., Fansuri, H., Widiastuti, N., Rahardjo, S.B. (2016). Solvothermal and electrochemical synthetic method of HKUST-1 and its methane storage capacity. IOP Conf. Ser.: Mater. Sci. Eng. 107, 012030. https://doi.org/10.1088/1757-899X/107/1/012030

Li, B.C., Lin, J.Y., Lee, J., Kwon, E., Thanh, B.X., Duan, X., Chen, H.H., Yang, H., Lin, K.Y.A. (2021).

Size-controlled nanoscale octahedral HKUST-1 as an enhanced catalyst for oxidative conversion of vanillic alcohol: The mediating effect of polyvinylpyrrolidone. Colloids Surf., A 631, 127639. https://doi.org/10.1016/j.colsurfa.2021.127639

Liu, Y., Liu, S., Gonçalves, A.A.S., Jaroniec, M. (2018). Effect of metal–ligand ratio on the CO_2 adsorption properties of Cu–BTC metal–organic frameworks. RSC Adv. 8, 35551–35556. https://doi.org/10.1039/C8RA07774F

Mahadi, N., Misran, H., Othman, S.Z. (2016). Synthesis and characterizations of MOF-199 using PODFA as porogen for CO_2 adsorption applications. Key Eng. Mater. 694, 44–49. https://doi.org/10.4028/www.scientific.net/KEM.694.44

McEwen, J., Hayman, J.D., Ozgur Yazaydin, A. (2013). A comparative study of CO_2, CH_4 and N_2 adsorption in ZIF-8, Zeolite-13X and BPL activated carbon. Chem. Phys. 412, 72–76. https://doi.org/10.1016/j.chemphys.2012.12.012

McKinstry, C., Cussen, E.J., Fletcher, A.J., Patwardhan, S. V., Sefcik, J. (2017). Scalable continuous production of high quality HKUST-1 via conventional and microwave heating. Chem. Eng. J. 326, 570–577. https://doi.org/10.1016/j.cej.2017.05.169

Morales, E.M.C., Méndez-Rojas, M.A., Torres-Martínez, L.M., Garay-Rodríguez, L.F., López, I., Uflyand, I.E., Kharisov, B.I. (2021). Ultrafast synthesis of HKUST-1 nanoparticles by solvothermal method: Properties and possible applications. Polyhedron 210, 115517. https://doi.org/10.1016/j.poly.2021.115517

Mosleh, S., Rahimi, M.R., Ghaedi, M., Dashtian, K., Hajati, S., Wang, S. (2017). Ag_3PO_4/AgBr/Ag-HKUST-1-MOF composites as novel blue LED light active photocatalyst for enhanced degradation of ternary mixture of dyes in a rotating packed bed reactor. Chem. Eng. Process. Process Intensif. 114, 24–38. https://doi.org/10.1016/j.cep.2017.01.009

Mu, X., Chen, Y., Lester, E., Wu, T. (2018). Optimized synthesis of nano-scale high quality HKUST-1 under mild conditions and its application in CO_2 capture. Microporous Mesoporous Mater. 270, 249–257. https://doi.org/10.1016/j.pnsc.2018.08.002

Nobar, S.N. (2018). Cu-BTC synthesis, characterization and preparation for adsorption studies. Mater. Chem. Phys. 213, 343–351. https://doi.org/10.1016/j.matchemphys.2018.04.031

Pan, R., Tang, Y., Guo, Y., Shang, J., Zhou, L., Dong, W., He, D. (2021). HKUST-1 and its graphene oxide composites: Finding an efficient adsorbent for SO_2 capture. Microporous Mesoporous Mater. 323, 111197. https://doi.org/10.1016/j.micromeso.2021.111197

Pioquinto-García, S., Rosas, J.M., Loredo-Cancino, M., Giraudet, S., Soto-Regalado, E., Rivas-García, P., Dávila-Guzmán, N.E. (2021). Environmental assessment of metal-organic framework DUT-4 synthesis and its application for siloxane removal. J. Environ. Chem. Eng. 9, 106601. https://doi.org/10.1016/j.jece.2021.106601

Salehi, S., Anbia, M. (2017). High CO_2 adsorption capacity and CO_2/CH_4 selectivity by nanocomposites of MOF-199. Energy Fuels 31, 5376–5384. https://doi.org/10.1021/acs.energyfuels.6b03347

Shang, S., Tao, Z., Yang, C., Hanif, A., Li, L., Tsang, D.C.W., Gu, Q., Shang, J. (2020). Facile synthesis of CuBTC and its graphene oxide composites as efficient adsorbents for CO_2 capture. Chem. Eng. J. 393, 124666. https://doi.org/10.1016/j.cej.2020.124666

Souza, B.E., Rudić, S., Titov, K., Babal, A.S., Taylor, J.D., Tan, J.C. (2019). Guest-host interactions of nanoconfined anti-cancer drug in metal-organic framework exposed by terahertz dynamics. Chem. Commun. 55, 3868–3871. https://doi.org/10.1039/C8CC10089F

Stawowy, M., Róziewicz, M., Szczepańska, E., Silvestre-Albero, J., Zawadzki, M., Musioł, M., Łuzny, R., Kaczmarczyk, J., Trawczyński, J., Łamacz, A. (2019). The Impact of synthesis method on the properties and CO_2 sorption capacity of UiO-66(Ce). Catalysts 9, 309. https://doi.org/10.3390/catal9040309

Thi, T.V.N., Luu, C.L., Hoang, T.C., Nguyen, T., Bui, T.H., Nguyen, P.H.D., Thi, T.P.P. (2013). Synthesis of MOF-199 and application to CO_2 adsorption. Adv. Nat. Sci.: Nanosci. Nanotechnol. 4, 35016. https://doi.org/10.1088/2043-6262/4/3/035016

Thommes, M., Kaneko, K., Neimark, A. V., Olivier, J.P., Rodriguez-Reinoso, F., Rouquerol, J., Sing, K.S.W. (2015). Physisorption of gases, with special reference to the evaluation of surface area and pore size distribution (IUPAC Technical Report). Pure Appl. Chem. 87, 1051–1069. https://doi.org/10.1515/pac-2014-1117

Wang, Y., Li, M., Hu, J., Feng, W., Li, J., You, Z. (2022). Highly efficient and selective removal of Pb^{2+} by ultrafast synthesis of HKUST-1: Kinetic, isotherms and mechanism analysis. Colloids
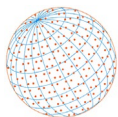
Surf., A 633, 127852. https://doi.org/10.1016/j.colsurfa.2021.127852

Wijaya, C.J., Ismadji, S., Aparamarta, H.W., Gunawan, S. (2021). Statistically optimum HKUST-1 synthesized by room temperature coordination modulation method for the adsorption of crystal violet dye. Molecules 26, 6430. https://doi.org/10.3390/molecules26216430

Yan, X., Komarneni, S., Zhang, Z., Yan, Z. (2014). Extremely enhanced CO_2 uptake by HKUST-1 metal-organic framework via a simple chemical treatment. Microporous Mesoporous Mater. 183, 69–73. https://doi.org/10.1016/j.micromeso.2013.09.009

Yang, M.W., Chen, N.C., Huang, C.H., Shen, Y.T., Yang, H.S., Chou, C.T. (2014). Temperature swing adsorption process for CO_2 capture using polyaniline solid sorbent. Energy Procedia 63, 2351–2358. https://doi.org/10.1016/j.egypro.2014.11.256

Ye, S., Jiang, X., Ruan, L.W., Liu, B., Wang, Y.M., Zhu, J.F., Qiu, L.G. (2013). Post-combustion CO_2 capture with the HKUST-1 and MIL-101(Cr) metal–organic frameworks: Adsorption, separation and regeneration investigations. Microporous Mesoporous Mater. 179, 191–197. https://doi.org/10.1016/j.micromeso.2013.06.007

Yulia, F., Utami, V.J., Nasruddin, Zulys, A. (2019). Synthesis, characterizations, and adsorption isotherms of CO_2 on chromium terephthalate (MIL-101) metal-organic frameworks (MOF). Int. J. Technol. 10, 1427–1436. https://doi.org/10.14716/ijtech.v10i7.3706

Zhao, Y., Cao, Y., Zhong, Q. (2014). CO_2 capture on metal-organic framework and graphene oxide composite using a high-pressure static adsorption apparatus. J. Clean Energy Technol. 2, 34–37. https://doi.org/10.7763/JOCET.2014.V2.86

Zhou, Z., Mei, L., Ma, C., Xu, F., Xiao, J., Xia, Q., Li, Z. (2016). A novel bimetallic MIL-101(Cr, Mg) with high CO_2 adsorption capacity and CO_2/N_2 selectivity. Chem. Eng. Sci. 147, 109–117. https://doi.org/10.1016/j.ces.2016.03.035